ORIGINAL ARTICLE

Deep learning-based earthquake catalog reveals the seismogenic structures of the 2022 M$_W$ 6.9 Chihshang earthquake sequence

Wei-Fang Sun[1], Sheng-Yan Pan[1], Chun-Ming Huang[1], Zhuo-Kang Guan[1], I-Chin Yen[2], Chun-Wei Ho[3], Tsung-Chih Chi[4], Chin-Shang Ku[4], Bor-Shouh Huang[4], Ching-Chou Fu[4] and Hao Kuo-Chen[1*]

Abstract

On 18 September 2022, the M$_W$ 6.9 Chihshang earthquake struck the south half of the Longitudinal Valley, Taiwan, and caused severe damage. A precise and rapid report for the distribution of aftershock sequence after a devastating earthquake provides key information for deciphering the seismogenic structure in the source region. The utilization of deep-learning methodologies for earthquake event detection offers a significant acceleration in data analysis. In this study, we use SeisBlue, a deep-learning platform/package, to extract the whole earthquake sequence from September to October 2022, including the M$_W$ 6.5 Guanshan foreshock, the M$_W$ 6.9 mainshock, over 14,000 aftershocks, and 866 foal mechanisms from two sets of broadband networks. After applying hypoDD for earthquakes, the distribution of aftershock sequence clearly depicts not only the Central Range Fault and the Longitudinal Valley Fault but also several local, shallow tectonic structures that have not been observed along the southern Longitudinal Valley.

Keywords 2022 M$_W$ 6.9 Chihshang earthquake sequence, SeisBlue, AI earthquake catalog, Seismogenic structure, Longitudinal Valley

1 Introduction

The Chihshang earthquake sequence began on 17 September 2022 with the M$_W$ 6.5 Guanshan earthquake (UTC 13:41:19.1) as the biggest foreshock, and 17 h later on 18 September 2022, the M$_W$ 6.9 mainshock (UTC 06:44:15.2) occurred. Both earthquakes contain reverse faulting with left-lateral movement on a west-dipping fault plane (Fig. 1). Due to the shallow depths (~7 km) of both strong earthquakes, catastrophic damages were caused along the southern Longitudinal Valley (LV) in eastern Taiwan (e.g. Central Geological Survey (CGS)

in Taiwan 2022; Chou et al. 2022; Ko et al. 2023). After the Guanshan foreshock occurred, a few damages were reported in the areas south of Guanshan in Taitung, and then the Chihshang mainshock induced severe damages distributed northward from Chihshang to Yuli and Rueisuei in southern Hualien. The spatial–temporal development of the damages follows the source rupture evolution of both earthquakes (Lee et al. 2023).

As an arc-continental collision environment, the LV represents the suture of the Eurasia and Philippine Sea Plates, which has the Central Range (CR), deformed passive Eurasian margin, to the west and the Coastal Range (CoR), northernmost tip of the Luzon Arc, to the east (Chang et al. 2000). According to the 30-year relocated earthquake catalog from the Central Weather Administration (CWA), Kuochen et al. (2004) and this study (Fig. 1) indicate that the southern segment (< 23.5ºN) of eastern Taiwan contains a major fault system dipping to the east beneath the LV because the Eurasia Plate

*Correspondence:
Hao Kuo-Chen
kuochenhao@ntu.edu.tw
[1] Department of Geosciences, National Taiwan University, No. 1. Sec. 4. Roosevelt Rd., Taipei 106, Taiwan
[2] YIC Geological Office, Penghu 880, Taiwan
[3] Seismological Center, Central Weather Administration, Taipei 100, Taiwan
[4] Institute of Earth Sciences, Academia Sinica, Taipei 115, Taiwan

Sun *et al. Terrestrial, Atmospheric and Oceanic Sciences*   (2024) 35:5

Page 2 of 16

subducts to the east under the Philippine Sea Plate. In 70 years after the great 1951 Hualien-Taitung earthquake sequence (Shyu et al. 2007; Chung et al. 2008), only two M6 + earthquakes occurred in the southern LV, the 2003 M_W 6.8 Chengkung and the 2006 M_W 6.1 Taitung earthquakes. In 2003, the M_W 6.8 Chengkung earthquake struck the east coast and triggered the majority of the aftershocks distributed to the east along the Coastal Range Fault (CoRF) (Kuochen et al. 2007) (also called the Chihshang Fault (CSF), the southern segment of the Longitudinal Valley Fault, LVF), and two small shallow clusters of the aftershocks are also found beneath the LV and CR to the west. Three years later, the M_W 6.1 Taitung earthquake occurred further southwest in the valley. This time only a few aftershocks were triggered along the CoRF at a deep depth of about 40 km, and the majority of the aftershocks were located to the west at a depth of 5–40 km along the Central Range Fault (CRF or CNF) (Shyu et al. 2006; Wu et al. 2006).

Seismology has been a data-driven research field. Over the past decade, the amount of data availability in seismology has grown enormously, through the large deployment of traditional sensors, dense nodal arrays, and distributed acoustic sensing (DAS) (Trugman et al. 2022). Due to the rapid growth of earthquake raw data and the vigorous development of machine learning tools, the application of machine learning technology in seismology has increased rapidly in recent years (Kong et al. 2019), and earthquake monitoring is one of the important tasks (Anikiev et al. 2023; Mousavi and Beroza 2023). Earthquake catalogs are essential benchmark datasets for seismological research and are used for earthquake source analysis, velocity models, seismotectonic interpretation, earthquake disaster prevention, etc. Combined with developed machine learning modules and/or traditional seismological tools, seismologists further construct machine learning-based workflows to obtain various archive earthquake catalogs (e.g. Jiang et al. 2022; Zhang et al. 2022; Yoon et al. 2023), or even automate the entire process or achieve real-time monitoring with cloud computing technology (Zhu et al. 2023).

In this study, we apply SeisBlue (Kuo-Chen et al. 2022; Huang et al. 2023), a deep learning-based platform for seismology, to a two-month (September–October 2022), 14-broadband-sation seismic datasets to extract the body-wave arrivals to build the detailed earthquake catalogs for revealing the seismogenic structures of the 2022 M_W 6.9 Chihshang earthquake sequence.

2 Data and analysis
2.1 The Chihshang seismic network and the combined waveform dataset
In November 2021, the Department of Geosciences of National Taiwan University and the Institute of Earth Sciences (IES) of Academia Sinica, Taiwan, deployed five permanent seismic stations (CS01-CS05 in Fig. 1) with station distances ranging from 10 to 25 km in the adjacent area of Chihshang, Taitung, as the Chihshang seismic network (CSN). The CSN is part of the project MAGIC (Multidimensional Active fault of Geo-Inclusive observatory Chihshang) for monitoring microseismicity at the creeping segment of the Chihshang Fault (CSF) (Angelier et al. 2000; Thomas et al. 2014; Harris 2017). The instruments are equipped with five broadband seismometers (Meridia Compact Posthole, Nanometrics Inc., Canada) with sampling rates of 100 Hz, and the real-time waveform files are transmitted to IES via 4G since June 2022.

The CSN greatly improve the earthquake detection ability for the 2022 Chihshang earthquake sequence because both the strong foreshock and mainshock occurred within the network (Fig. 1). For the first day after the M_W 6.5 foreshock occurred, most earthquakes located within the CSN (Fig. 2c), and later the M_W 6.9 mainshock triggered aftershocks expanded outside the CSN northward and southward (Fig. 2d-f). To keep the two-month earthquake catalog as complete as possible, we tested a dataset of 40 broadband seismic stations from the Broadband Array in Taiwan for Seismology (BATS, Institute of Earth Sciences, Academia Sinica, Taiwan 1996) for better station coverage. We found that nine out of 40 BATS stations are mostly selected into the earthquake catalog, so we collected data from the nine BATS stations with the five CSN stations (Fig. 1) as the combined waveform dataset used in this study.

2.2 SeisBlue
To extract the earthquake catalog, we apply the deep learning-based package for seismology, SeisBlue (Kuo-Chen et al. 2022; Huang et al. 2023), to both the CSN and BATS datasets of continuous waveform files. The architecture of SeisBlue consists of three stages:

(See figure on next page.)
Fig. 1 Background seismicity of the eastern Taiwan. The black rectangular is the study area. The cooper color-coded circles are the 3D-hypoDD-relocated M3 + CWA catalog from 2001 to 2020. The rainbow color-coded starts are M6 + earthquakes since 2018. The two beach balls represent the focal mechanisms of the M_W 6.5 Guanshan foreshock and M_W 6.9 Chihshang mainshock of the 2022 Chihshang earthquake sequence. Red triangles and squares are permanent broadband seismic stations of the CSN and BATS networks, respectively. Red traces are active faults mapped by CGS (Lin et al. 2021). GS: Guanshan; CS: Chihshang
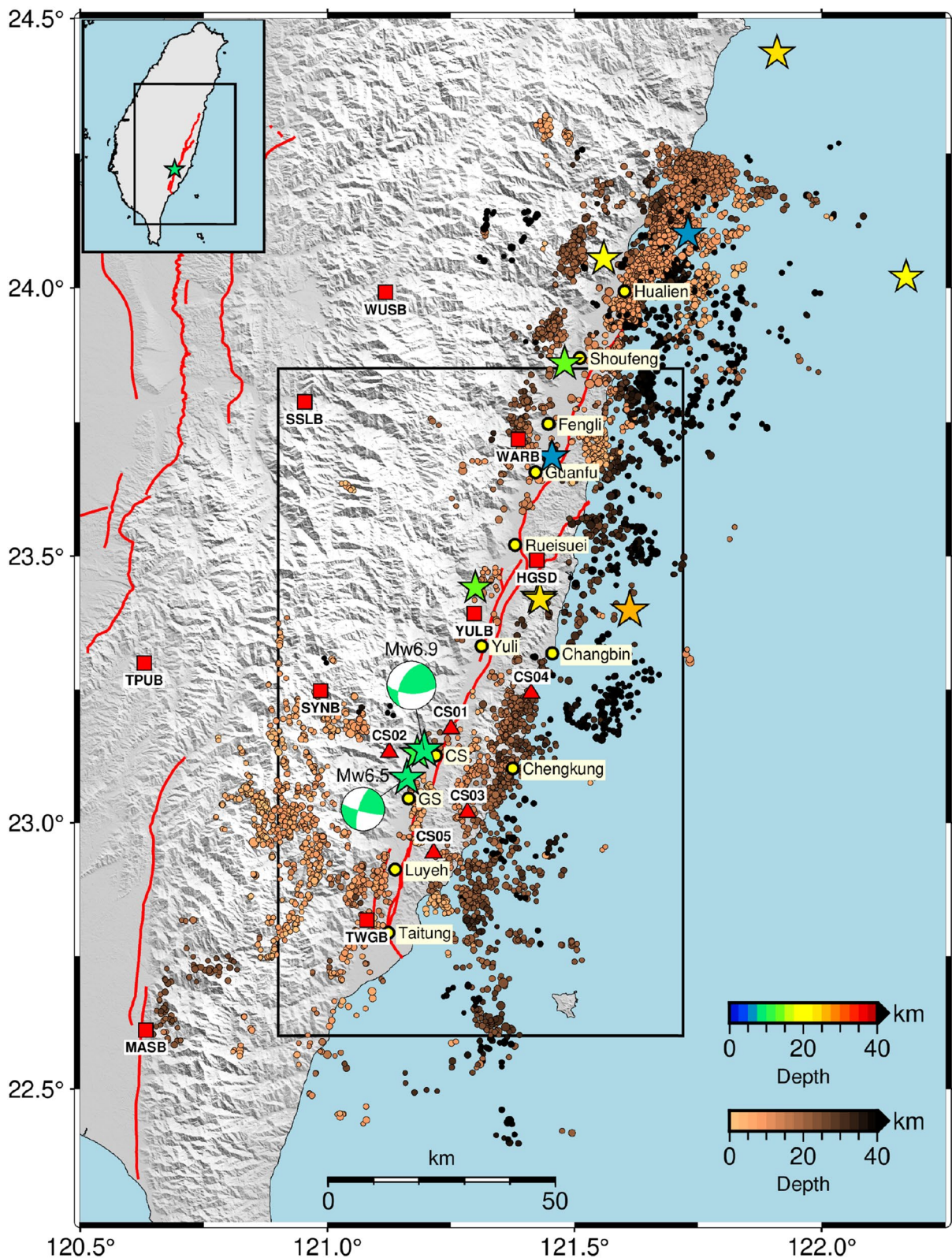
Fig. 1 (See legend on previous page.)

Sun *et al. Terrestrial, Atmospheric and Oceanic Sciences*   (2024) 35:5
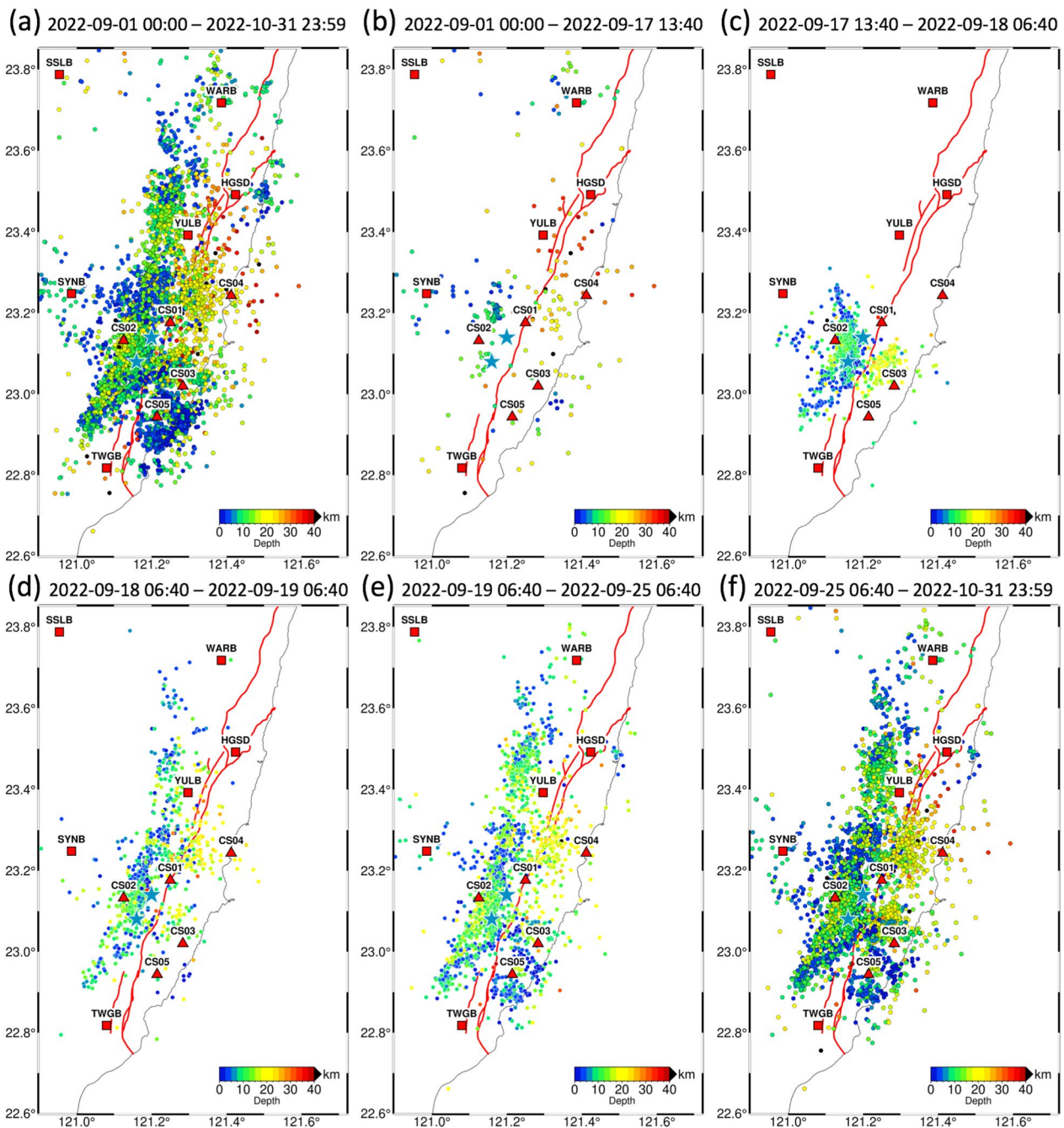
Page 4 of 16

Fig. 2 Seismicity evolution during the 2022 M_W 6.9 Chihshang earthquake sequence. **a** All events for two months from September to October 2022, **b** events before the M_W 6.5 foreshock, **c** events between the M_W 6.5 foreshock and the M_W 6.9 mainshock, **d** events within 1 day after the mainshock, **e** events within 2nd–7th days after the mainshock, and **f** events 7 days after the mainshock until 31 October 2022. The rainbow color-coded circles and starts are seismicity and the Guanshan foreshock and Chihshang mainshock, respectively. Red triangles and squares are permanent broadband seismic stations of the CSN and BATS networks, respectively. The red traces are active faults mapped by CGS (Lin et al. 2021)

preprocessing, model prediction, and postprocessing (Fig. 3a). Preprocessing prepares data, model prediction utilizes deep learning models, and post-processing derives insights. The architecture is modularized to embrace future changes and to ensure an efficient code structure by incorporating principles such as abstraction, information hiding, module independence, and clear interfaces. The data processing pipeline is modularized
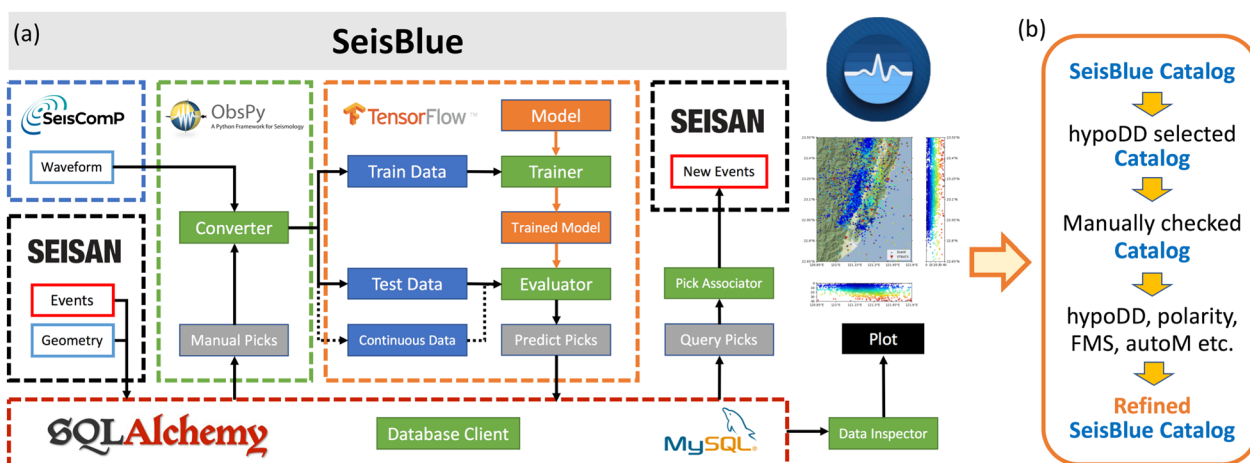
Fig. 3 Workflow to generate the refined 2022 M_W 6.9 Chihshang earthquake catalog. **a** The architecture of the deep learning-based SeisBlue platform. **b** The subsequent data processing procedures to obtain the refined SeisBlue earthquake catalog

for code reusability, ease of testing, and independent development. This architecture optimizes data processing, prediction, and insight derivation, while the modular design and relational database enhance robustness and scalability.

The procedure achieved by SeisBlue for retrieving near real-time or off-line earthquake catalog includes receiving real-time waveform data from seismic station via seedlink or archive, preprocessing data, auto detecting phase arrivals, auto associating and locating events, listing events into catalog, and visualizing data (Fig. 3a). The two essential modules in SeisBlue are the deep learning models for seismic phase detection and associator for grouping valid phase arrivals into each single seismic event. To date, the deep learning models used in SeisBlue modified from PhaseNet (Zhu and Beroza 2019) and EQ-Transformer (Mousavi et al. 2020), and the associator is adapted from PhasePAPY (Chen and Holland 2016). PhaseNet (Zhu and Beroza 2019) utilizes the U-net architecture for seismic phase detection, EQ-Transformer (Mousavi et al. 2020) employs the Transformer architecture for earthquake signal processing, and SeisBlue enhances training through the integration of generative adversarial models with seismic data. These models are trained on a local seismic dataset of Taiwan, and their performance is evaluated using testing data from the same dataset, simulating real-time scenarios. The incorporation of diverse models and seismic datasets contributes to improved accuracy and efficiency in earthquake detection and signal processing. PhasePAPY (Chen and Holland 2016) identifies clusters of arrival times during rough localization, focusing on those with similar origin times based on the S-P time estimation theory (Havskov and Ottemöller 2010). After removing outliers of arrival

times, precise earthquake localization is implemented by the HYPOCENTER program (Lienert and Havskov 1995) integrated in SEISAN (Havskov and Ottemöller 1999; Havskov et al. 2020) and then listed as earthquake catalog reports.

Software development of SeisBlue follows version control with GitHub (https://github.com/SeisBlue/SeisBlue), Docker containerization, and CI/CD for efficient collaboration, deployment, and automation. These integrated technologies and practices revolutionize seismic event detection and monitoring, improving accuracy, efficiency, and real-time analysis for scientific and community-based initiatives.

2.3 The SeisBlue catalog and the refined SeisBlue catalog

SeisBlue can efficiently obtain earthquake catalog from continuous seismic waveform data (e.g. Kuo-Chen et al. 2022). However, our goal for the AI catalog of the 2022 M_W 6.9 Chihshang earthquake sequence is not only extracting as many seismic events as possible but also other physical parameters of the seismic sources, such as focal mechanism solution (FMS) and earthquake magnitude, which rely on accurate phase arrival data. In this study, we further process the SeisBlue AI earthquake catalog (SeisBlue catalog in short afterward) (Fig. 3a) through three steps to obtain the refined SeisBlue catalog (Fig. 3b). Firstly, we apply the hypoDD program (Waldhauser and Ellsworth 2000) to the SeisBlue catalog for extracting events which have both similar locations and phase arrival combinations (Fig. 4b) to obtain the hypoDD-selected SeisBlue catalog. Secondly, we visually inspect the hypoDD-selected events by cross checking the raw 3-component waveforms with the picks generated by SeisBlue and mark the P-wave polarities, and
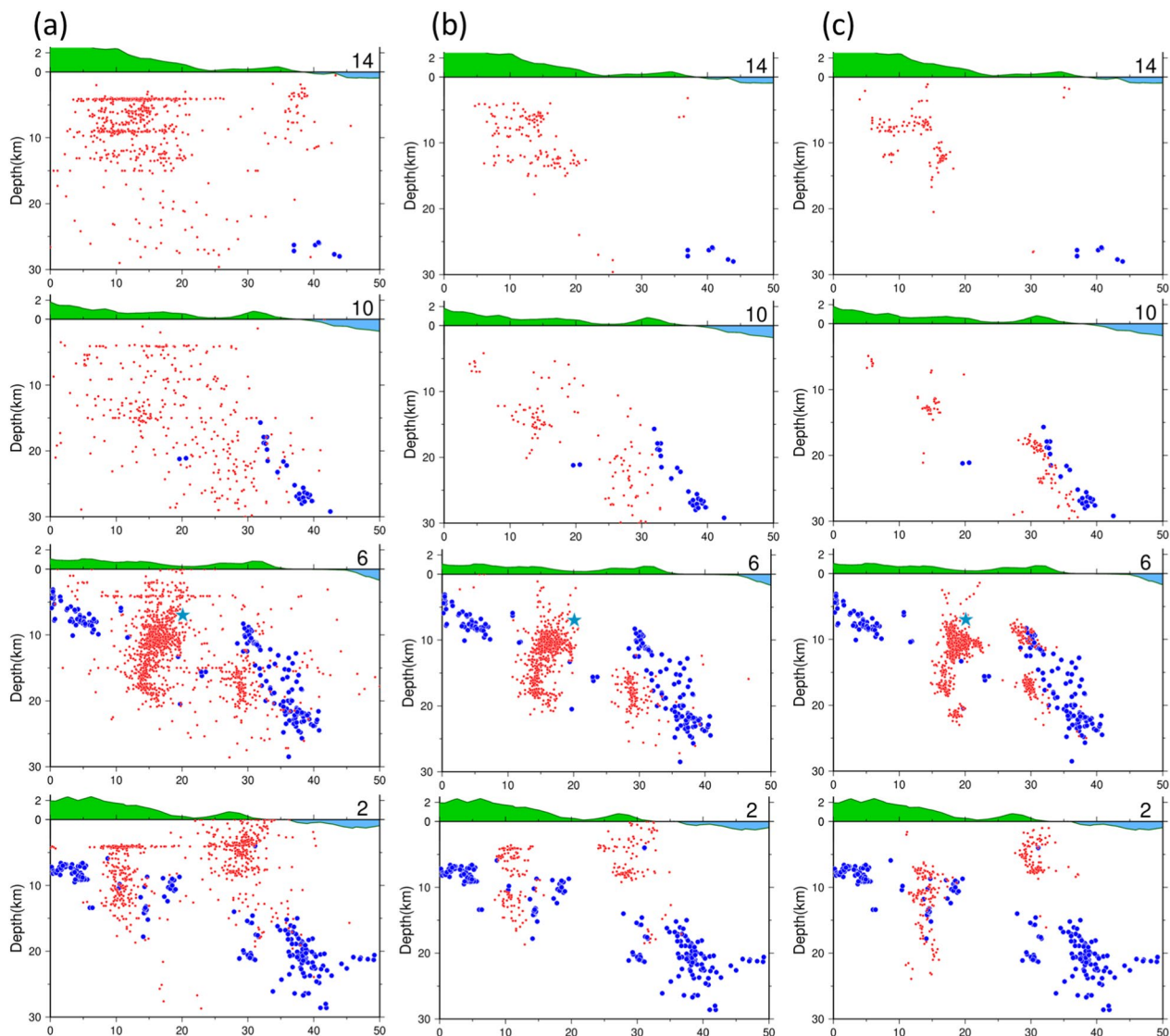
Fig. 4 Profiles of different selected seismicity of the 2022 M_W 6.9 Chihshang earthquake sequence. The red dots are seismicity of **a** the SeisBlue catalog located by HYPOCENTER, **b** the hypoDD-selected SeisBlue catalog, and **c** the hypoDD-relocated SeisBlue catalog. The blue circles are seismicity of the 3D-hypoDD-relocated M3 + CWA catalog from 2001 to 2020. The traces in each upper panel represent topography. The locations of profiles can be referred to Fig. 7 with the profile numbers. The profile width is ± 3 km

then the manually checked SeisBlue catalog is created. In the last step, we apply several seismological programs integrated in SEISAN (Havskov and Ottemöller 1999; Havskov et al. 2020) to obtain FMS and earthquake magnitudes and form the refined SeisBlue catalog.

SEISAN, the seismic data processing software SeisAn Earthquake analysis software (Havskov and Ottemöller 1999; Havskov et al. 2020), is mainly used for analysis of seismic wave arrival time selection, earthquake location, earthquake magnitude, P-wave polarities and FMS. In this study, we use several seismological programs modified and integrated in SEISAN, such as

HYPOCENTER, hypoDD, FPFIT, and auto magnitude (Ottemöller et al. 2021). The SeisBlue catalog is located by the HYPOCENTER program (Lienert and Havskov 1995) with a Taiwan 1-D velocity model (Chen and Shin 1998) (e.g. Fig. 4a, b). We apply the hypoDD program (Waldhauser and Ellsworth 2000) to the SeisBlue catalog to improve relative locations in clusters of seismic events and obtain the relocated SeisBlue catalog (e.g. Fig. 4c). We use the FPFIT program (Reasenberg 1985) to determine the double couple earthquake FMS using the manually picked P-wave polarities. The advantage of FPFIT is that formal errors are estimated and only

one solution is given (Reasenberg 1985). Moment Magnitude (M_W) is determined by using spectral analysis (Havskov and Ottemöller 2010; Holt et al. 2021) with a 1D attenuation model from Chen et al. (1996) and Chen (1998). Local magnitude (M_L) is calculated following the Richter's original formula (Richter 1935) revised for Taiwan (Shin 1993; Guan et al. 2020), as implemented by SEISAN (Havskov and Ottemöller 1999; Havskov et al. 2020). Seismic waveform amplitudes are defined after removing instrument response, simulating a Wood-Anderson instrument. The M_W/M_L are considered at least three M_W/M_L readings have been obtained for each earthquake.

3 Results

3.1 The SeisBlue catalog

For monitoring microseismicity on the creeping Chihshang Fault system and due to the sparse distribution of seismic station in the eastern Taiwan, we deployed the CSN in early November 2021 to increase station coverage. The 2022 M_W 6.9 Chihshang earthquake sequence happens to prove our thought. Without the CSN data, SeisBlue detects 6924 earthquakes using the continuous seismic data from the nine BATS stations during September to October 2022 (Fig. 5a). However, because the strongest foreshock and the mainshock occurred within the CSN, SeisBlue detects 14,454 earthquakes by combining the CSN and BATS datasets (Fig. 5b). Especially
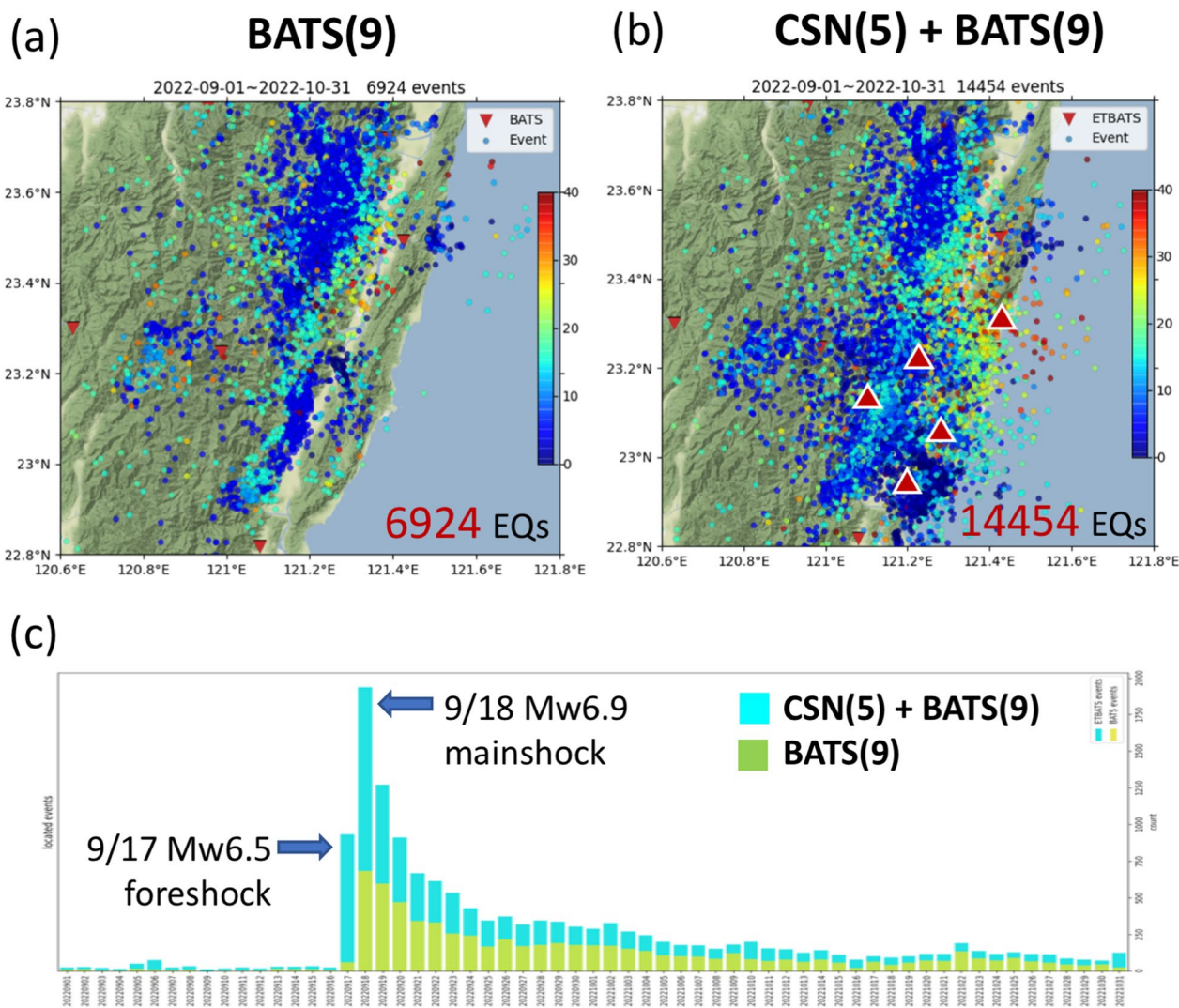

Fig. 5 Comparison of SeisBlue catalogs using different continuous seismic waveform datasets. Map view of the two-month seismicity: **a** Using nine BATS stations only and **b** using nine BATS and five CSN stations. Number of earthquakes is indicated in the map. The rainbow-colored circles indicate seismic events, inverted triangles BATS stations, and triangles CSN stations. **c** Daily earthquake number of the two catalogs

on 17 September 2022 when the strong M_W 6.5 foreshock occurred, SeisBlue detects ~100 events without the CSN data but over 800 events with it (Fig. 5c). The earthquake detection ability is greatly improved by the CSN dataset.

Taking 3 stations and a total number of 6 P- and S-wave arrivals as the minimum criteria to locate a single seismic event, the SeisBlue catalog contains 14,276 earthquakes (Fig. 6b) with 64,266 P- and 61,785 S-wave arrivals from September to October 2022. During the same time period and geographical range, the CWA (Central Weather Administration, CWA, Taiwan 2012) catalog lists 1427 seismic events (Fig. 6a). We simply define a match between a CWA catalog event and a Seis-Blue catalog event if their origin times matched within 1 s. SeisBlue contains 755 matching events, misses 492 CWA events, and adds 13,521 new events.

Before the M_W 6.5 foreshock occurred, tens of small foreshocks clustered in the Guanshan and Chihshang area and also small earthquakes in other places in the eastern Taiwan (Fig. 2b). After the M_W 6.5 foreshock occurred in Guanshan, earthquakes were all concentrated in the Guanshan and Chihshang area (Fig. 2c). Then the stronger M_W 6.9 mainshock struck northward in Chihshang and triggered ruptures not only in the foreshock-mainshock area but also northward to Yuli and Rueisuei, Hualien and southward to Luyeh, Taitung (Fig. 2d–f).

3.2 The refined SeisBlue catalog

We used the hypoDD program (Waldhauser and Ellsworth 2000) to improve relative locations in clusters of seismic events (Fig. 4) and extract those 5,691 events (Figs. 7a and 8) from the SeisBlue catalog of 14,276 events (Fig. 6b). Then we visually inspected
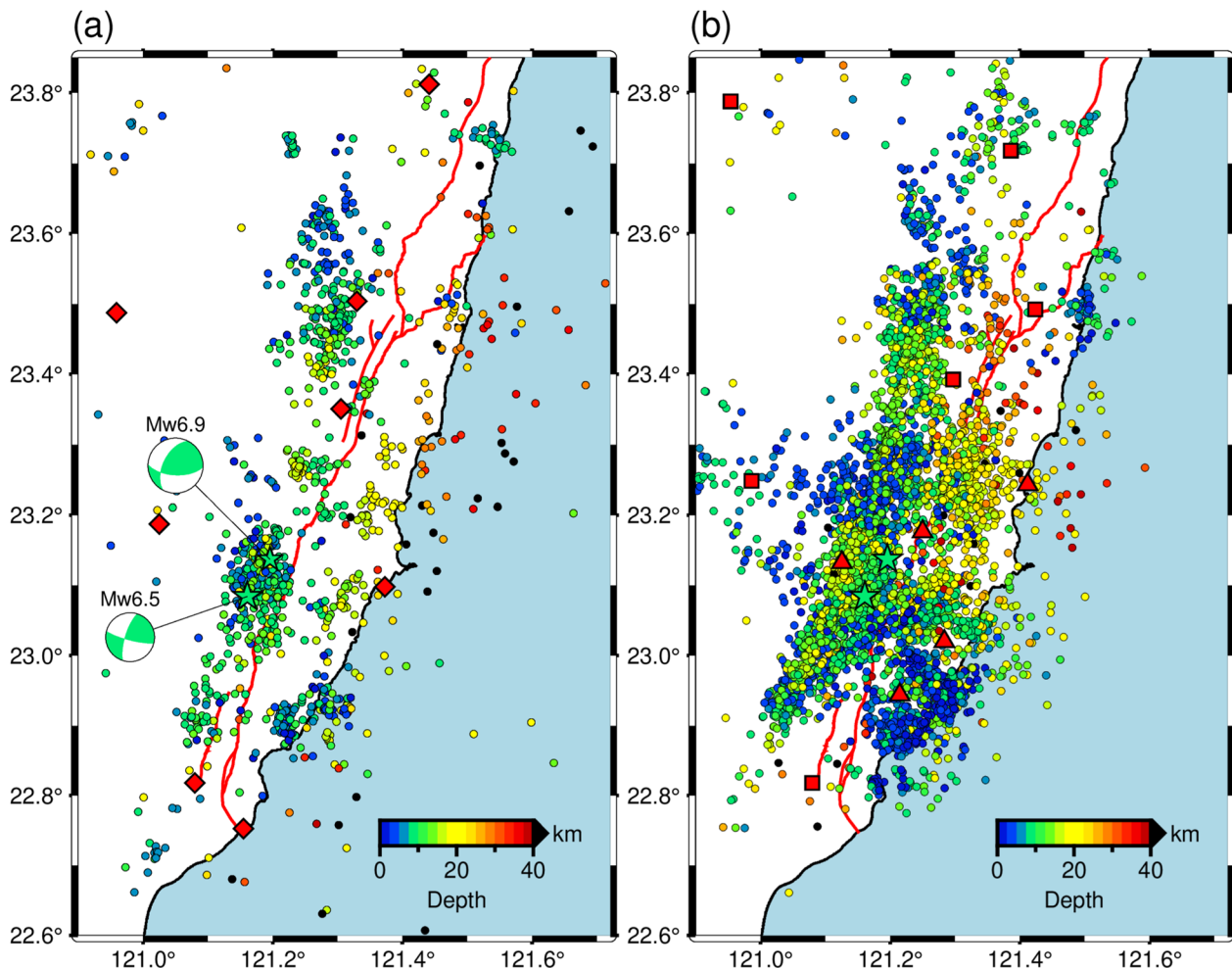

Fig. 6 Two-month seismicity of the 2022 M_W 6.9 Chihshang earthquake sequence of **a** CWA and **b** SeisBlue (this study). The rainbow color-coded circles and starts are seismicity and the Guanshan foreshock and Chihshang mainshock, respectively. Red diamonds, triangles and squares are permanent short period or broadband seismic stations of the CWA, CSN and BATS networks, respectively. Red traces are active faults mapped by CGS (Lin et al. 2021)
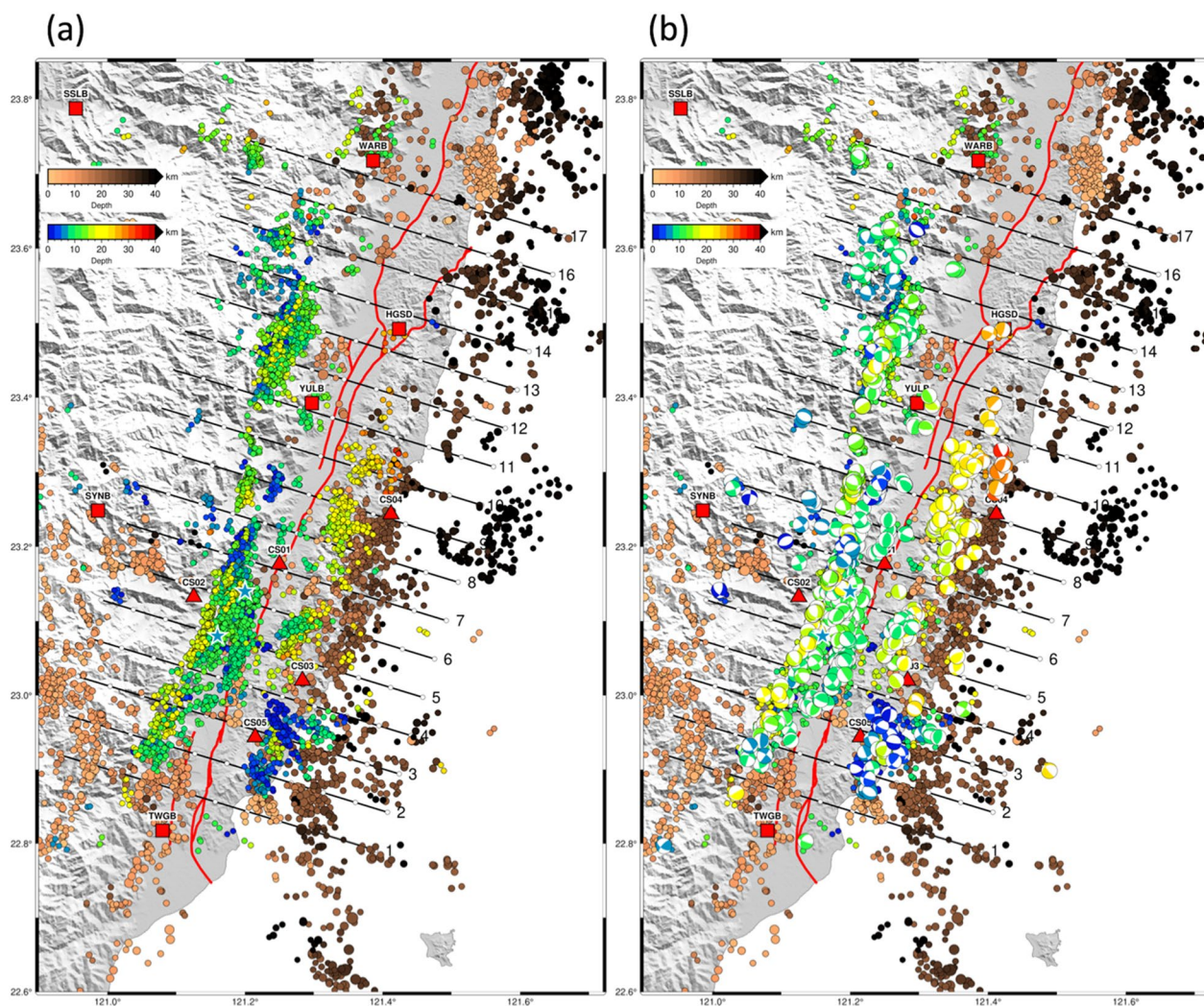
Fig. 7 **a** Seismicity and **b** focal mechanisms of the hypoDD-relocated SeisBlue catalog of the 2022 M_W 6.9 Chihshang earthquake sequence. The cooper color-coded circles are the 3D-hypoDD-relocated M3+CWA catalog from 2001 to 2020. The rainbow-color coded circles and beach balls are seismicity and focal mechanisms of the relocated SeisBlue catalog. The black lines with numbers 2–16 are locations for profiles in Figs. 4, 8 and 9. Each profile is 6 km apart and the profile width is ± 3 km. The Red traces are active faults mapped by CGS (Lin et al. 2021)

the 5,691 hypoDD-selected events by cross checking the raw 3-component waveforms with the picks generated by SeisBlue and manual marked the P-wave polarities. In total, all 5691 events passed the quality control step with 32,522 SeisBlue P-wave, 31,523 SeisBlue S-wave, 12,889 manual P-wave, and 12,198 manual S-wave arrivals, and 8,834 up- and 8,843 down P-wave polarities. 782 and 486 false positives for P- and S-wave arrivals marked by SeisBlue are checked and removed. We located all 5691 events by HYPO-CENTER with the renewed P- and S-wave arrivals and removed events with location error in depth ≤ 10 km to form the hypoDD-selected SeisBlue catalog consisting of 5,151 events. The root-mean-square (RMS) of the

travel time residuals and standard errors in the epicenter (ERH), in the depth (ERZ), and in the longitude (ERX) of the hypoDD-selected SeisBlue catalog are 0.324 ± 0.080 s, 3.322 ± 1.435 km, 4.143 ± 1.898 km, and 2.662 ± 1.248 km, respectively.

We used the P-wave polarities of the 14 broadband stations and the FPFIT program (Reasenberg 1985), which using grid search method, to obtain the best fit FMS for each event by at least six readings of P-wave polarity. In total 1,629 FMSs can be determined from the P-wave polarity data and we then selected 866 FMS with F ≤ 0.1 (F-factor, 0–1, one-norm misfit function. F < 0.5 for good fit and F = 1.0 for perfect misfit) and errors of strike, dip and rake are all < 20°, respectively (Figs. 7b and 9).
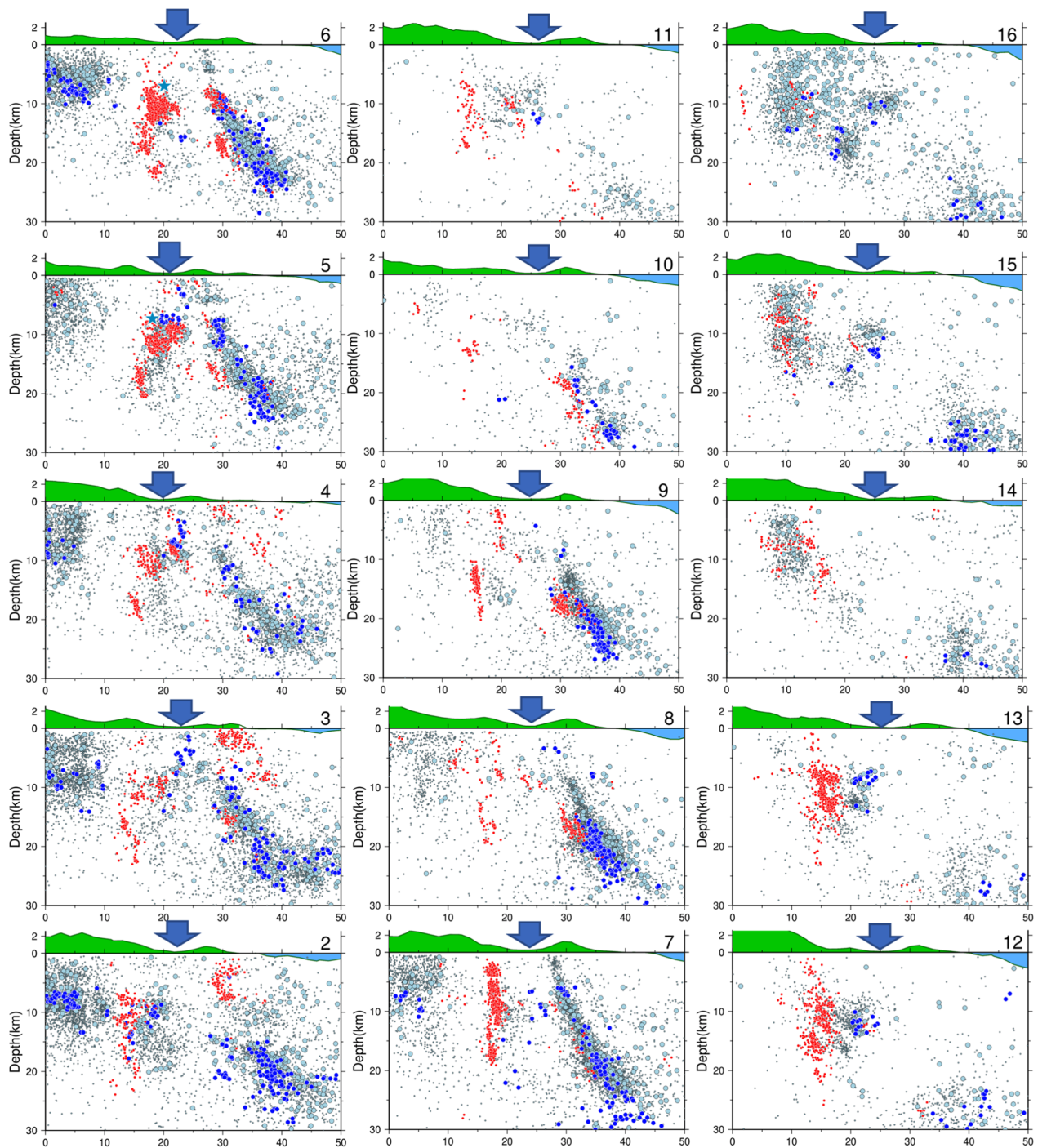
Fig. 8 Profiles of seismicity of the hypoDD-relocated SeisBlue catalog of the 2022 M_W 6.9 Chihshang earthquake sequence. The red, blue, light blue circles are seismicity of the hypoDD-relocated SeisBlue catalog from September to October 2022, the 3D-hypoDD-relocated M3 + CWA catalog from 2001 to 2020, and the 3D relocated CWA catalog from 1990 to 2017 from Wu et al. (2008), respectively. In upper panels, the traces represent topography, and the blue arrows denote the location of the LV. The locations of profiles can be referred to Fig. 7 with the profile numbers. Each profile is 6 km apart and the profile width is ± 3 km
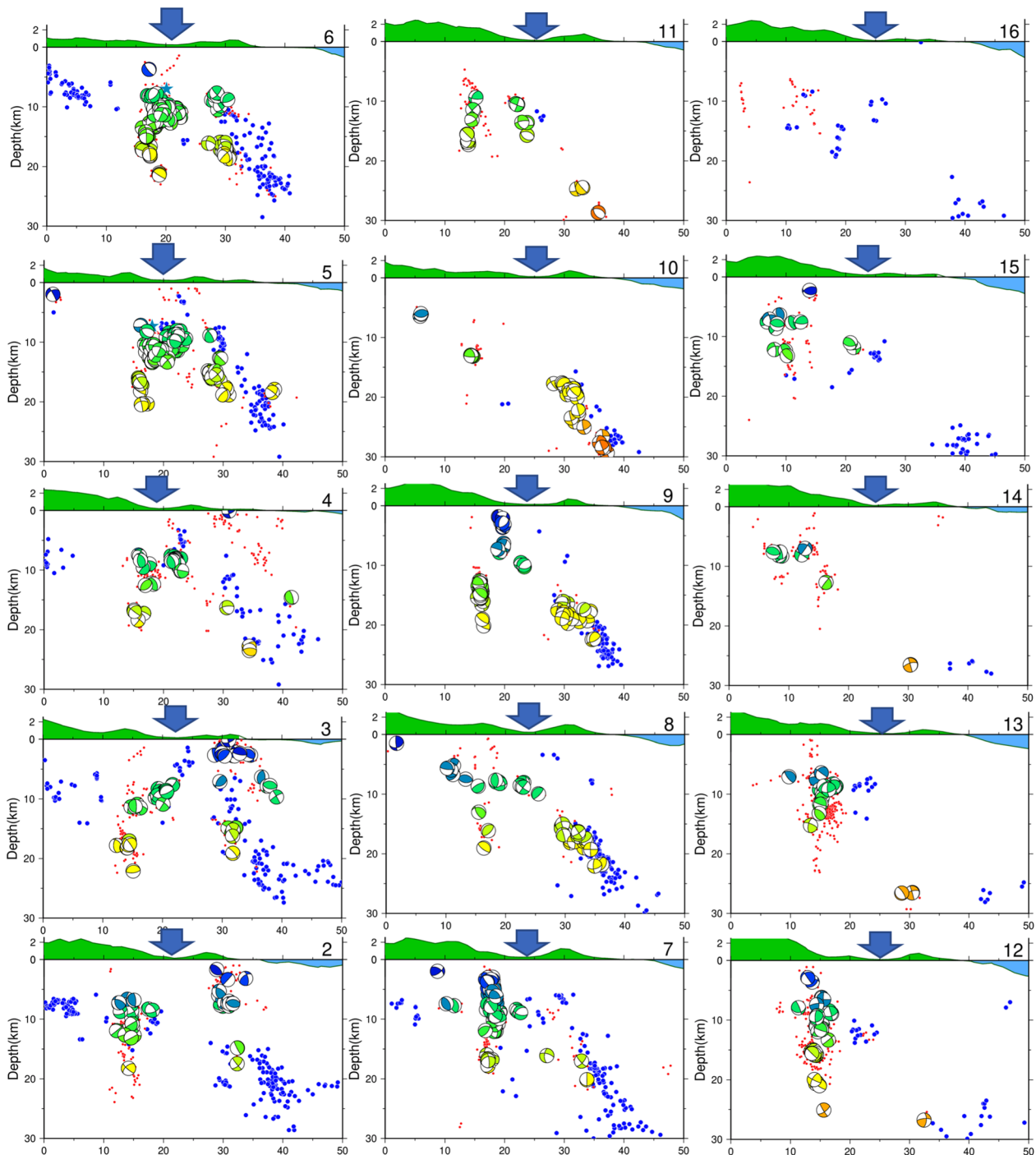
Fig. 9 Profiles of the focal mechanisms of the hypoDD-relocated SeisBlue catalog of the 2022 M_W 6.9 Chihshang earthquake sequence. The rainbow-color coded beach balls are focal mechanisms. The red and blue circles are seismicity of the hypoDD-relocated SeisBlue catalog from September to October 2022 and the 3D-hypoDD-relocated M3 + CWA catalog from 2001 to 2020, respectively. In upper panels, the traces represent topography, and the blue arrows denote the location of the LV. The locations of profiles can be referred to Fig. 7 with the profile numbers. Each profile is 6 km apart and the profile width is ±3 km
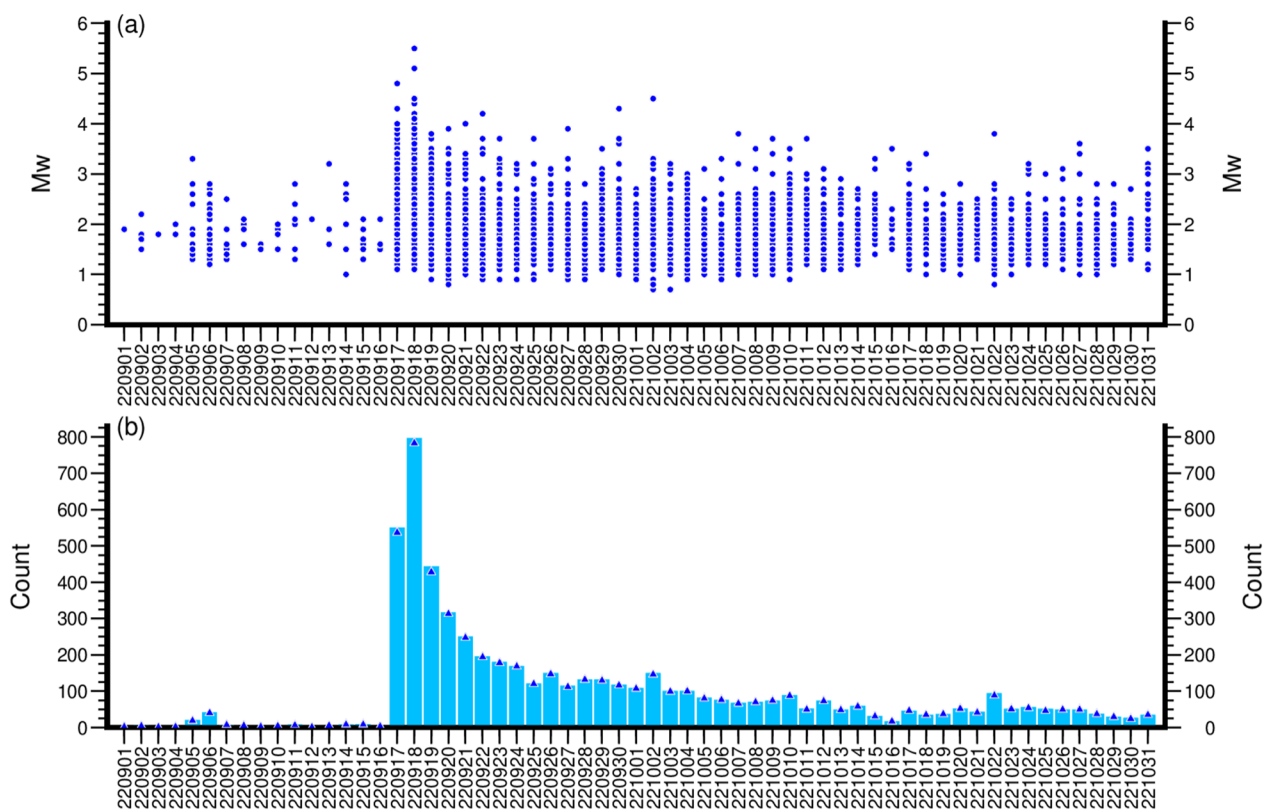
Fig. 10 Daily distributions of **a** M_W and **b** numbers of earthquake (blue bars) and M_W (dark blue triangles) of the refined SeisBlue catalog of the 2022 M_W 6.9 Chihshang earthquake sequenc

The local magnitude (M_L) and moment magnitudes (M_W) are automatically determined by SEISAN and then checked and revised by analysts. Both the M_L and M_W for each earthquake was averaged by at least three readings. The semi-automatic earthquake magnitude procedure can obtain reliable M_W values according to the temporal evolution of the foreshock-mainshock-aftershock sequence (Fig. 10a, b). The relation between M_L and M_W in this study has a soft transition from 1:1 for $M_L > 4$ to 2/3 between $1 < M_L < 4$, which fits the theoretical prediction in Deichmann (2017) (Fig. 11a). The magnitude of completeness of M_L and M_W in this study are about 0.8 and 1.6, respectively (Fig. 11b). From the comparison between M_L / M_W obtained in this study with the M_W catalog from BATS (autoBATS, Jian et al. 2018) and the M_L catalog from CWA (GDMS, Central Weather Administration, CWA, Taiwan 2012), we found systematically differences among them that (1) the M_W / M_L of this study and the M_W of autoBATS are in the relation of 1:1 but the M_L are $\sim$ 0.1–0.5 less than the M_W of auto-BATS (Fig. 11c); (2) the M_L in this study and the M_L of GDMS are in the relation of 1:1 too but M_L in this study are $\sim$ 0.5–1.0 less than the M_L of GDMS (Fig. 11d); and (3) the relation between the M_L of GDMS and the M_W in

this study is similar to that between M_L and M_W in this study (Fig. 11a, d).

Based on the combined seismicity of the relocated CWA catalog for the past three decades (Wu et al. 2008) and our refined SeisBlue catalog of the 2022 M_W 6.9 Chihshang earthquake sequence, we can find several seismogenic characteristics in southeast Taiwan. First, the LVF on land is an east-dipping system from Luyeh to Yuli (section 2–11, Figs. 8 and 9), whose depth can extend from more than 30 km to almost to the surface beneath the CoR, which can be seen clearly the most in section 7 (Chihshang-Chengkung). Second, a small cluster of seismic events beneath the southernmost CoR at shallow depth less than 5 km was triggered by the mainshock and stayed active for more than two months. This cluster is clearly not part of the LVF system because of its location and FMSs (section 2–4, Figs. 8 and 9). On the other hand, under the CR to the west, the fault structures are more complicated. Here we divide the seismogenic structures into three groups: (a) section 2–6; (b) section 7–9; and (c) section 11–13 (Figs. 8 and 9). In group (a) at depth of 15–25 km, we can see a clear east-dipping seismicity. There are two groups of seismicity at depth of 2–15 km. To the west, a steeper east-dipping seismicity located at
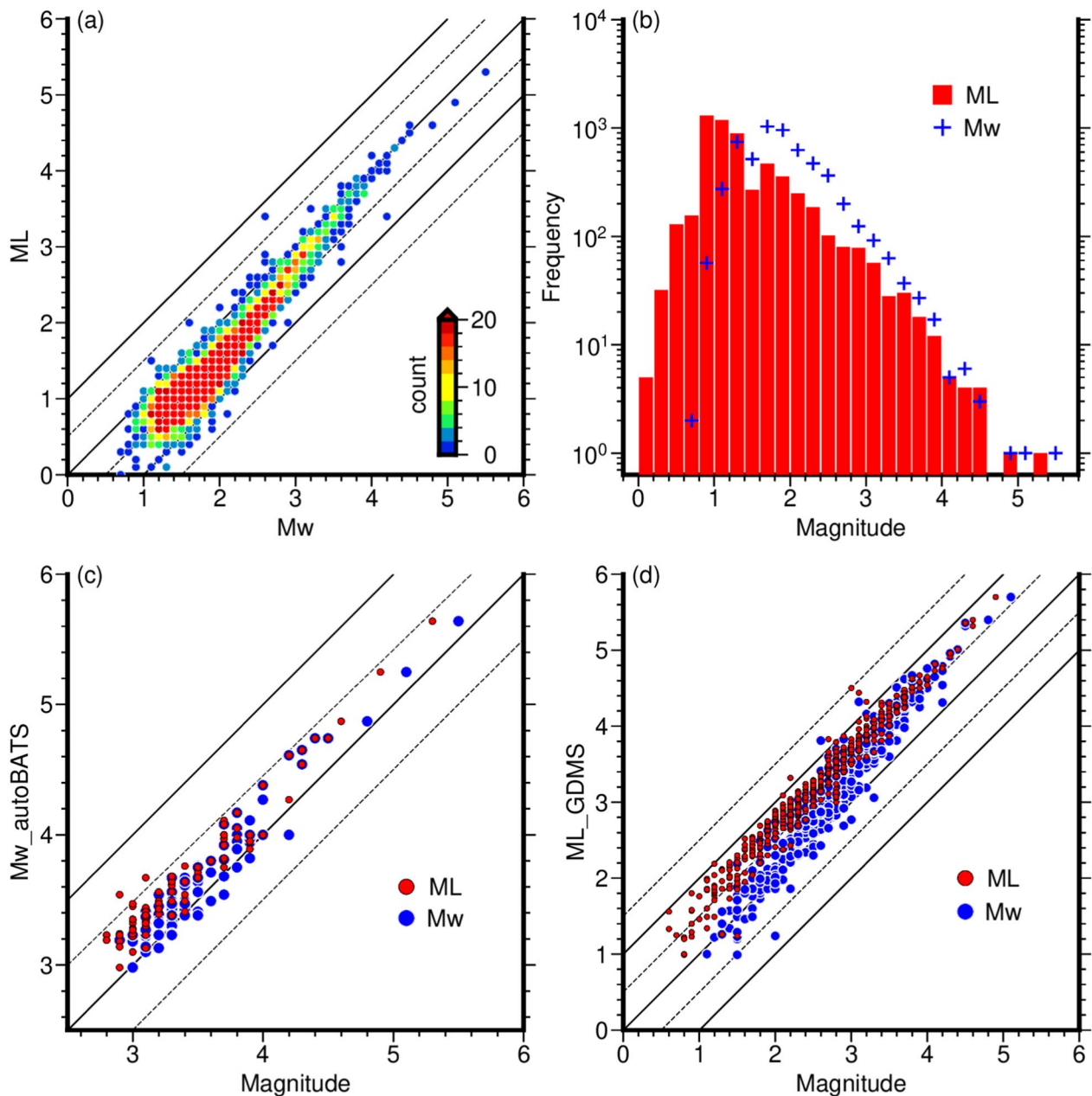
Fig. 11 Earthquake magnitude of the refined SeisBlue earthquake catalog. **a** M_L versus M_W; **b** earthquake magnitude-frequency distribution; **c** M_W of autoBATS (Jian et al. 2018) and **d** M_L of CWA versus both M_L and M_W, respectively

depth of 5–15 km. To the east, a west-dipping seismicity at depth of 2–15 km extents westward and seems to connect to the LVF system, especially in section 5–6 (Figs. 8 and 9). In group (b) an east-dipping seismicity also can been seen but at shallower depth of 10–20 km, and it turns almost perpendicular at depth 0–10 km in section 7 (Figs. 8 and 9), and a few unclear branches at depth of 0–10 km in section 8 and 9 (Figs. 8 and 9). There is a seismic gap under the CR in section 10. In group

(c) between Yuli (section 11) and Rueisuei (section 13) the east-dipping seismicity moves westward at depth of 5–25 km. The seismicity beneath the CR is not concentrated further north in section 14–16 (Figs. 8 and 9).

4 Discussion
The aim of this study is to use the refined SeisBlue AI earthquake catalog, extracted from a dataset of dense broadband seismic networks installed near the 2022 M_W

6.9 Chihshang mainshock area, to explain the seismogenic structures of the southern segment of the LV. Therefore, the process of analyzing earthquake location is relatively simplified, so conventional locating methods/processes are not used, such as obtaining a new reliable 1D velocity model, using existing 3D velocity models, or using various absolute or relative relocation methods (e.g. Zhang et al. 2022). By comparing with the earthquake catalog of the CWA, the credibility and reliability of the SeisBlue catalog is tested. Furthermore, relative location methods, such as hypoDD, are less dependent on the velocity model and can obtain high location resolution of clusters of earthquakes (Waldhauser and Ellsworth 2000). Compared with the relocated earthquake catalog in the past 30 years (Kuochen et al. 2004; Wu et al. 2008), our relocated SeisBlue catalog is consistent with the seismic events that occurred before but more active, the shallow swarm at the southernmost tip of the CoR, and further represent the unseen near-vertically distributed seismicity beneath the CR from Luyeh to Chihshang and from Yuli to Rueisuei. Kuo-Chen et al. (2023) surveyed eight new reflection seismic profiles along the LV and found that the west-dipping CRF does not exist along the west side of the LV at least at a depth of 1 to 2 km. Combined with the 30-year background seismicity, the reflection seismic profiles, and our refined SeisBlue catalog, we can infer that several near-vertical fault segments more than 10 km long exist under the CR with a depth of 2–20 km and this deeply buried fault system extends at least 70 km from Yuli to Luyeh.

The completeness of the understanding of regional seismogenic structures depends on sufficient observation network(s) and the occurrence of large earthquake(s). In recent years, powerful AI tools have become more and more essential to consume the increasing amount of seismic data (e.g. Yoon et al. 2023 and the references therein). For example, in 1951, an M7.1 and an M6.8 earthquake occurred near Yuli and Chihshang (Chung et al. 2008), respectively, but due to the lack of sufficient seismic networks, we could obtain the source characteristics of the mainshocks (e.g. Chung et al. 2008) but not the aftershock sequences for analyzing the seismogenic structures. Most studies of the seismotectonics in eastern Taiwan mainly focus on the LVF system (e.g. Thomas et al. 2014) because most recorded M7+earthquakes occurred there and sparse observation network in the CR due to terrain restrictions. Combining with the previously mentioned advantages, our results show that the clear seismogenic structures beneath the CR and the LVF and CRF systems do have interactions beneath the LV in the mainshock source area.

The tectonic structure of eastern Taiwan has been studied by different disciplines, especially for the evolution of the oblique collision between the Luzon arc and the passive Eurasia Plate from regional scale (e.g. Chang et al. 2000) to lithospheric scale (e.g. Malavieille and Trullenque 2009; Shyu et al. 2011; Zhang et al. 2020; Lai et al. 2022). The buried forearc basement due to the shortening of the Luzon forearc lithosphere is shown among those lithospheric scale models of the southern LV (e.g. Malavieille and Trullenque 2009; Shyu et al. 2011; Zhang et al. 2020; Lai et al. 2022). The deformation of the accretionary wedge forearc basin may be the key to the complex seismogenic structures beneath the CR compared to that beneath the CoR. According to the geological model of Lai et al. (2022), at the narrow transection of the LV at a width of less than 30 km, the tectonic units contain, from west to east, metamorphism, mélange, arc crust, volcanic rocks, and sedimentary rocks at depth from 0 to 40 km that makes the seismicity complicated.

Shyu et al. (2011) used the arrival data of two earthquake sequences of the 2003 M_W 6.8 Chengkung and the 2006 M_W 6.1 Taitung earthquakes recorded by the CWA seismic network to obtain a 3D travel-time tomography and proposed a lithospheric scale model of the southern LV. The 2022 Chihshang earthquake sequence is more widely distributed than the two earthquake sequences in Taitung and is well recorded by dense broadband seismic networks (CSN and BATS) and a denser nodal array in the Guanshan-Chihshang area. Combining these two seismic data sets with SeisBlue, we believe that the future completion of a new high-resolution (~1 km) version of travel-time tomography will enhance our understanding of the seismotectonic and seismogenic structures of the southern LV.

5 Conclusion

Although the 2022 M_W 6.9 Chihshang earthquake sequence is not the biggest earthquake occurred in the southeast Taiwan, but it is the first M6+earthquake well recorded by the dense broadband array and detected by a deep leaning-based seismological platform, SeisBlue. The refined and relocated SeisBlue catalog shows that the 2022 Chihshang earthquake sequence filled several seismic gaps which have not been observed clearly in eastern Taiwan for the past 30 years: (1) along the CR at a depth of 1–25 km and developed several branches eastward beneath LV at a depth of 1–10 km; (2) along the west side of CoR on CoRF at a depth of 10–25 km; and (3) at the southernmost tip of CoR, east of CoRF at a shallow depth of 0–5 km. A small cluster of earthquakes occurred on 5–6 September 2022 at the mainshock area; after the M_W 6.5 Guanshan earthquake, as the strongest foreshock, occurred on 7 September 2022, most seismicity concentrated in the foreshock-mainshock area for a day, and then the mainshock triggered several clusters northward

to Yuli and Rueisuei in Hualien, southward to Luyeh in Taitung, and eastward along the CoR.

Author contributions
Conceptualization: HK, CF, IY, and WS. Methodology: WS, SP, CMH, ZG, CWH, and HK. Formal analysis: WS, SP, and CWH. Data collection and fieldwork: WS, TC, and CK. Supervision: HK, CF, and BH. Writing—original draft: WS. Writing—review and editing: WS, IY, and HK.

Data availability
The refined SeisBlue catalog of the 2022 Chihshang earthquake sequence, which contains 5,151 seismic events with event time, hypoDD location, local and moment magnitudes, and focal mechanism, can be provided based on request. Please contact Sun WF via ttsun.sun@gmail.com.

Declarations

Competing interests
The authors declare that they have no competing interests.

References
Angelier J, Chu HT, Lee JC, Hu JC (2000) Active faulting and earthquake hazard: the case study of the Chihshang fault, Taiwan. Jx Geodyn 29(3–5):151–185

Anikiev D, Birnie C, Bin Waheed U, Alkhalifah T, Gu C, Verschuur DJ, Eisner L (2023) Machine learning in microseismic monitoring. Earth Sci Rev 239:104371

Central Geological Survey in Taiwan (2022). 2022 Chihshang Earthquake Sequence Geological Survey Report (in Chinese). https://faultnew. moeacgs.gov.tw/Reports/More/63cc5a4b2020403d9f79d3c33a7aba0c. Accessed 22 Aug 2023

Central Weather Administration (CWA, Taiwan) (2012) Central weather administration seismographic network. Int Feder Dig Seismogr Netw. https://doi.org/10.7914/SN/T5

Chang CP, Angelier J, Huang CY (2000) Origin and evolution of a melange: the active plate boundary and suture zone of the Longitudinal Valley, Taiwan. Tectonophysics 325(1–2):43–62

Chen KJ (1998) S-wave attenuation structure in the Taiwan area and its correlation to seismicity. Terr Atmos Ocean Sci 9:97–118. https://doi.org/10.3319/tao.1998.9.1.97(t)

Chen C, Holland AA (2016) PhasePApy: a robust pure Python package for automatic identification of seismic phases. Seismol Res Lett 87(6):1384–1396

Chen YL, Shin TC (1998) Study of the earthquake location of 3-D velocity structure in Taiwan area. Meteorol Bull 42:135–169

Chen KJ, Yeh YH, Shyu CT (1996) Qp structure in the Taiwan area and its correlation to seismicity. Terr Atmos Ocean Sci 7:409–429. https://doi.org/10.3319/TAO.1996.7.4.409(ACCT)

Chou CC, Wu CL, Chai JF, Yao GC (2022) Reconnaissance report on seismic damage caused by Guanshan earthauke and Chihshang earthquake, Taiwan, 2022 V3.0, National Center for Research on Earthquake Engineer.

https://www.ncree.narl.org.tw/assets/file/20220918_EQ_NCREE_V3.0.pdf. Accessed 22 Aug 2023

Chung LH, Chen YG, Wu YM, Shyu JB, Kuo YT, Lin YN (2008) Seismogenic faults along the major suture of the plate boundary deduced by dislocation modeling of coseismic displacements of the 1951 M7. 3 Hualien-Taitung earthquake sequence in eastern Taiwan. Earth Planet Sci Lett 269(3–4):416–426

Deichmann N (2017) Theoretical basis for the observed break in M_L/M_W scaling between small and large earthquakes. Bull Seismol Soc Am 107(2):505–520

Guan ZK, Kuo-Chen H, Sun WF (2020) Re-calculation of the attenuation functions for local magnitude from the upgraded central weather bureau seismic network in Taiwan. TAO Terr Atmos Ocean Sci. 31(4):4

Harris RA (2017) Large earthquakes and creeping faults. Rev Geophys 55(1):169–198

Havskov J, Ottemöller L (1999) SeisAn earthquake analysis software. Seismol Res Lett 70:532–534. https://doi.org/10.1785/gssrl.70.5.532

Havskov J, Ottemöller L (2010) Routine data processing in earthquake seismology. Springer, Dordrecht. https://doi.org/10.1007/978-90-481-8697-6

Havskov J, Voss PH, Ottemöller L (2020) Seismological observatory software: 30 yr of seisan. Seismol Res Lett 91:1846–1852. https://doi.org/10.1785/0220190313

Holt J, Whidden KM, Koper KD, Pankow KL, Mayeda K, Pechmann JC, Edwards B, Gök R, Walter WR (2021) Toward robust and routine determination of M_W for small earthquakes: application to the 2020 M_W 5.7 Magna, Utah, seismic sequence. Seismol Res Lett 92(2A):725–740

Huang CM, Chang LH, Kuo-Chen H, Zhuang Y (2023) SeisBlue: a deep-learning data processing platform for seismology. EGU General Assembly, Vienna, pp 24–28. https://doi.org/10.5194/egusphere-egu23-13927 (**EGU23-13927**)

Institute of Earth Sciences, Academia Sinica, Taiwan (1996) Broadband array in Taiwan for seismology. Institute of Earth Sciences, Academia Sinica, Taipei City. https://doi.org/10.7914/SN/TW

Jian PR, Tseng TL, Liang WT, Huang PH (2018) A new automatic full waveform regional moment tensor inversion algorithm and its applications in the Taiwan area. Bull Seismol Soc Am 108(2):573–587

Jiang C, Zhang P, White MC, Pickle R, Miller MS (2022) A detailed earthquake catalog for Banda Arc-Australian plate collision zone using machine-learning phase picker and an automated workflow. Seism Rec 2(1):1–10

Ko YY, Tsai CC, Hwang JH, Hwang YW, Ge L, Chu MC (2023) Failure of engineering structures and associated geotechnical problems during the 2022 M_L 6.8 Chihshang earthquake, Taiwan. Nat Hazards. 118:1–40

Kong Q, Trugman DT, Ross ZE, Bianco MJ, Meade BJ, Gerstoft P (2019) Machine learning in seismology: turning data into insights. Seismol Res Lett 90(1):3–14

Kuochen H, Wu YM, Chang CH, Hu JC, Chen WS (2004) Relocation of the Eastern Taiwan earthquakes and its tectonic implications. Terr Atmos Ocean Sci. 15:647–666. https://doi.org/10.3319/TAO.2004.15.4.647(T)

Kuochen H, Wu YM, Chen YG, Chen RY (2007) 2003 M_W6.8 Chengkung earthquake and its related seismogenic structures. J Asian Earth Sci. 31(3):332–339

Kuo-Chen H, Sun W, Huang C, Pan S (2022) Near real-time seismic data processing helps scientist understand aftershocks. Temblor. https://doi.org/10.32858/temblor.276

Kuo-Chen H, Brown D, Lai SY, Chen JY (2023) Reflection seismic profiling along the Longitudinal Valley Basin, Eastern Taiwan: in search of the Central Range fault. Tectonophysics 869:230129

Lai LSH, Dorsey RJ, Horng CS, Chi WR, Shea KS, Yen JY (2022) Extremely rapid up-and-down motions of island arc crust during arc-continent collision. Commun Earth Environ 3(1):100

Lee SJ, Liu TY, Lin TC (2023) The role of the west-dipping collision boundary fault in the Taiwan 2022 Chihshang earthquake sequence. Sci Rep 13(1):3552

Lienert BR, Havskov J (1995) A computer program for locating earthquakes both locally and globally. Seismol Res Lett 66(5):26–36

Lin CW, Liu YC, Chou PS, Lin YH (2021) Recent development of active fault investigations of Taiwan. Bull Centr Geol Surv 34:1–40

Malavieille J, Trullenque G (2009) Consequences of continental subduction on forearc basin and accretionary wedge deformation in SE Taiwan: Insights from analogue modeling. Tectonophysics 466(3–4):377–394

Mousavi SM, Beroza GC (2023) Machine learning in earthquake seismology. Annu Rev Earth Planet Sci 51:105–129

Mousavi SM, Ellsworth WL, Zhu W, Chuang LY, Beroza GC (2020) Earthquake transformer—an attentive deep-learning model for simultaneous earthquake detection and phase picking. Nat Commun 11(1):3952

Ottemöller L, Voss PH, Havskov J (2021) SEISAN earthquake analysis software for Windows, Solaris, Linux and Macosx, Version 12.0. University of Bergen, Bergan, p 607 (**ISBN 978-82-8088-501-2**)

Reasenberg PA (1985) FPFIT, FPPLOT, and FPPAGE: Fortran computer programs for calculating and displaying earthquake fault-plane solutions. US Geol. Surv Open-File Rep., pp 85–739

Richter CF (1935) An instrumental earthquake magnitude scale. Bull Seismol Soc Am 25(1):1–32

Shin TC (1993) The calculation of local magnitude from the simulated Wood-Anderson seismograms of the short-period seismograms in the Taiwan area. Terr Atmos Ocean Sci 4(2):155–170

Shyu JBH, Sieh K, Chen YG, Chung LH (2006) Geomorphic analysis of the Central Range fault, the second major active structure of the Longitudinal Valley suture, eastern Taiwan. Geol Soc Am Bull 118(11–12):1447–1462

Shyu JBH, Chung LH, Chen YG, Lee JC, Sieh K (2007) Re-evaluation of the surface ruptures of the November 1951 earthquake series in eastern Taiwan, and its neotectonic implications. J Asian Earth Sci 31(3):317–331

Shyu JBH, Wu YM, Chang CH, Huang HH (2011) Tectonic erosion and the removal of forearc lithosphere during arc-continent collision: Evidence from recent earthquake sequences and tomography results in eastern Taiwan. J Asian Earth Sci 42(3):415–422

Thomas MY, Avouac JP, Champenois J, Lee JC, Kuo LC (2014) Spatiotemporal evolution of seismic and aseismic slip on the Longitudinal Valley Fault, Taiwan. J Geophys Res Solid Earth 119(6):5114–5139

Trugman DT, Fang L, Ajo-Franklin J, Nayak A, Li Z (2022) Preface to the focus section on big data problems in seismology. Seismol Res Lett 93:2423–2425. https://doi.org/10.1785/0220220219

Waldhauser F, Ellsworth WL (2000) A double-difference earthquake location algorithm: method and application to the northern Hayward fault, California. Bull Seismol Soc Am 90(6):1353–1368

Wessel P, Luis JF, Uieda L, Scharroo R, Wobbe F, Smith WHF, Tian D (2019) The generic mapping tools version 6. Geochem Geophys Geosyst 20:5556–5564. https://doi.org/10.1029/2019GC008515

Wu YM, Chen YG, Chang CH, Chung LH, Teng TL, Wu FT, Wu CF (2006) Seismogenic structure in a tectonic suture zone: with new constraints from 2006 M_W6. 1 Taitung earthquake. Geophys Res Lett. https://doi.org/10.1029/2006GL027572

Wu YM, Chang CH, Zhao L, Teng TL, Nakamura M (2008) A comprehensive relocation of earthquakes in Taiwan from 1991 to 2005. Bull Seismol Soc Am 98(3):1471–1481

Yoon C, Cochran ES, Vanacore EA, Huerfano V, Báez-Sánchez G, Wilding JD, Smith J (2023) A detailed view of the 2020–2023 Southwestern Puerto Rico Seismic sequence with deep learning. Bull Seismol Soc Am. https://doi.org/10.1785/0120220229

Zhang Y, Tsai CH, Froitzheim N, Ustaszewski K (2020) The Yuli Belt in Taiwan: part of the suture zone separating Eurasian and Philippine Sea plates. Terr Atmos Ocean Sci 31(4):415

Zhang M, Liu M, Feng T, Wang R, Zhu W (2022) LOC-FLOW: an end-to-end machine learning-based high-precision earthquake location workflow. Seismol Res Lett 93:2426–2438. https://doi.org/10.1785/0220220019

Zhu W, Beroza GC (2019) PhaseNet: a deep-neural-network-based seismic arrival-time picking method. Geophys J Int 216(1):261–273

Zhu W, Hou AB, Yang R, Datta A, Mousavi SM, Ellsworth WL, Beroza GC (2023) QuakeFlow: a scalable machine-learning-based earthquake monitoring workflow with cloud computing. Geophys J Int 232(1):684–693

Publisher's Note